Compact Spoof Surface Plasmon Polariton Waveguides With Simple Configurations and Good Performance

Sen Lu, *Student Member, IEEE*, Kai-Da Xu, *Senior Member, IEEE*, Ying-Jiang Guo, *Member, IEEE*, and Qiang Chen, *Senior Member, IEEE*

***Abstract*— Two compact spoof surface plasmon polariton (SSPP) waveguides are proposed with simple configurations and good performance. Compared with the conventional SSPP structure having same asymptotic frequency, a new design of the tilted-stub structure occupies less transversal space. Moreover, this design can be applied in the SSPP cases with small period values, which will facilitate the longitudinal miniaturization. Then, an improved SSPP structure is constructed to realize the transversal size reduction of 58% compared with the conventional corrugated SSPP waveguide. For these two proposed waveguides, smooth transitions from microstrip lines to SSPPs are designed with seamless connection. Two experimental prototypes have been fabricated, whose measurements are in good agreement with the simulated ones. The proposed designs will have significant potentials for the miniaturization of plasmonic devices and circuits.**

***Index Terms*— Miniaturization design, spoof surface plasmon polaritons (SSPPs), transversal size reduction.**

I. Introduction

SURFACE plasmon polaritons (SPPs) are a class of surface waves propagating along the metal–dielectric interface with exponential decay in the vertical direction to the interface [1]. Due to the ability of strong field confinement, SPPs are well researched and developed at optical band [2]–[4]. At terahertz and microwave regimes, an SPP-like surface modes, namely spoof SPPs (SSPPs), are proposed to reproduce the properties of SPPs [5]. The SSPPs are constructed by adding periodic patterns on conductors, which can be tailored by changing the geometrical dimensions of the periodic structures [6], [7].

In order to make good use of such SSPP technology, numerous planar SSPP-based devices are implemented that can be conveniently integrated into the wireless communication systems, including filters [8]–[15], antennas [16]–[19], splitters [20], [21], phase shifters [22], matching loads [23], and so on. These SSPP-based devices possess the advantages of strong field confinement and ease of frequency manipulation that facilitates their applications in different scenarios.

For realizing lower asymptotic frequency and stronger field confinement, the groove of the SSPP periodic array always requires to be deeper. However, this will lead to large transversal size and sacrifice volume occupation. Hence, several efforts have been made to miniaturize the SSPP structures, which are all realized through structure deformations, such as split-ring grooves [24], spiral-shaped lines [25], T-shaped lines [26], meander lines [27], [28], and double-sided parallel-strip lines [29]. Especially in [24], due to the suitable configuration, the transition part can be avoided that decreases the longitudinal length as well. In [30], a new SSPP transmission line by loading capacitive metal strips realizes the size reduction and enhanced field confinement. In order to achieve deep upper frequency suppressions, two new SSPP structures using bow-tie unit cells are designed in [14] and [15]. However, these deformations of the SSPP structures make the configuration complicated and design time-consuming. Also, it usually occupies a relatively large longitudinal size for a period of SSPP unit cell.

In this article, two compact SSPP waveguides using simple configurations are proposed with transversal size reductions and good performance. First, by rotating the two-side stubs of the conventional corrugated SSPP structure, a new stub-tilted SSPP structure is constructed. This method is suitable to apply in the SSPP cases with small period values, thereby miniaturizing the longitudinal size. Then, to further decrease asymptotic frequency of the SSPP waveguide, an improved one is introduced, while its transversal size almost remains unchanged. The simulated and measured results, exhibiting low insertion loss (IL) and deep stopband suppression, validate the proposed ideas.

Manuscript received March 18, 2021; revised May 25, 2021, July 24, 2021, and September 24, 2021; accepted October 27, 2021. Date of publication November 10, 2021; date of current version December 17, 2021. This work was supported in part by the NSAF Joint Fund under Grant U2130102, in part by the Natural Science Foundation of Shaanxi Province of China under Grant 2021JQ-060, and in part by the "Siyuan Scholar" Fellowship of XJTU. The review of this article was arranged by Senior Editor J. G. Leopold. *(Corresponding author: Kai-Da Xu.)*

Sen Lu was with the Department of Electronic Science, Xiamen University, Xiamen 361005, China. He is now with the State Key Laboratory of Millimeter Waves, School of Information Science and Engineering, Southeast University, Nanjing 210096, China.

Kai-Da Xu is with the School of Information and Communications Engineering, Xi'an Jiaotong University, Xi'an 710049, China, and also with the Department of Communications Engineering, Tohoku University, Sendai 980-8579, Japan (e-mail: kaidaxu@ieee.org).

Ying-Jiang Guo is with the Microsystem and Terahertz Research Center, China Academy of Engineering Physics, Chengdu 610200, China.

Qiang Chen is with the Department of Communications Engineering, Tohoku University, Sendai 980-8579, Japan.

Color versions of one or more figures in this article are available at https://doi.org/10.1109/TPS.2021.3124045.

Digital Object Identifier 10.1109/TPS.2021.3124045

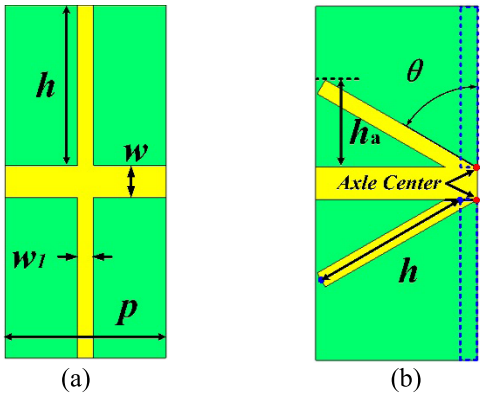

Fig. 1. Schematic configurations of (a) conventional corrugated SSPP unit cell and (b) proposed stub-tilted SSPP unit cell. The detailed dimensions are $p = 5$ mm, $w = 1$ mm, $h = 5$ mm, and $w_1 = 0.5$ mm.

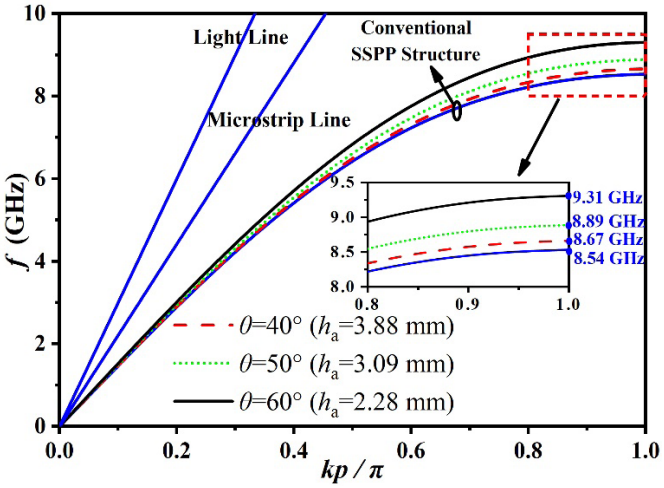

Fig. 2. Dispersion curves for the stub-tilted SSPP structure as a function of θ. The other parameters are $p = 5$ mm, $w = 1$ mm, $h = 5$ mm, and $w_1 = 0.5$ mm.

II. SSPP Waveguides

A. Stub-Tilted SSPP Structure With Transversal Size Reduction

Fig. 1 shows two SSPP unit cells where the yellow regions represent the metallic conducting strips attaching on the dielectric substrate. The back of the substrate is the metallic ground plane, which is in order to improve the electromagnetic field confinement and achieve lower asymptotic frequency. Fig. 1(a) illustrates the diagram of the conventional two-side corrugated SSPP unit cell, where the period, conducting strip width, height and width of each transversal stub are denoted as p, w, h, and w_1, respectively. Fig. 1(b) depicts the schematic of the proposed stub-tilted SSPP unit cell, where the transversal size occupation is reduced. It is constructed through the following two steps. First, moving the stubs of conventional SSPP unit cell to the right end (the blue dashed region), which will hardly influence its dispersion characteristics due to the periodic configuration. Second, rotating the bilateral stubs a certain angle symmetrically, i.e., θ, along the red points in Fig. 1(b). As for the tilted stub, its transversal size occupation is reduced from h to h_a.

With the help of the eigenmode solver in commercial software, we investigate the dispersion characteristics of the proposed stub-tilted SSPP structure (i.e., periodic array of the stub-tilted SSPP unit cell) with different θ, and its counterpart (conventional corrugated SSPP structure), as shown in Fig. 2. Also, the dispersion curves of the light line and microstrip line are introduced for references. Since the transversal size reduction is not obvious if the rotating angle is small, only the cases of large θ (40°, 50°, and 60°) are explored. In simulation, the substrate Rogers 5880 ($\varepsilon_r = 2.2$, $\tan\delta = 0.0009$) is used with a thickness of 0.508 mm. Seen from Fig. 2, the dispersion curve of the stub-tilted SSPP structure starts from the intersection with the light line and microstrip line, and then gradually deviates from them to the asymptotic frequency. With the deviation, the strong field confinement and low asymptotic frequency are both realized. However, the asymptotic frequencies of the stub-tilted SSPP structure (8.67, 8.89, and 9.31 GHz when $\theta = 40°$, $\theta = 50°$, and $\theta = 60°$, respectively) are all slightly higher than that of the conventional SSPP structure (8.54 GHz). This phenomenon is mainly caused by the effect of the reduced effective length as stub rotates, and this effect becomes obvious as θ increases. It should be noted that the spatial occupation of the bilateral stubs, i.e., h_a, reduces to 3.88, 3.09, and 2.28 mm, respectively, in these three rotating cases.

As the bilateral stubs tilt, the asymptotic frequency will be slightly increased. However, under the condition of same asymptotic frequency, the stub-tilted SSPP structure occupies greatly less lateral space compared with the conventional SSPP structure. A comparison is made below in detail. For stub-tilted SSPP structures in the cases of $\theta = 40°$, $\theta = 50°$, and $\theta = 60°$, their transversal dimensions ($2h_a + w$) are 8.98, 7.81, and 6.43 mm with corresponding asymptotic frequencies of 8.67, 8.89, and 9.31 GHz, respectively. However, for the conventional SSPP structures with these three different asymptotic frequencies, the corresponding transversal sizes ($2h + w$) will be 10.68, 10.28, and 9.64 mm, respectively. Therefore, it is found that the stub-tilted SSPP structures in these three cases can achieve the transversal size reductions of 16%, 24%, and 33%, respectively.

Based on the proposed stub-tilted SSPP unit cell of $\theta = 60°$, a SSPP waveguide (SSPP waveguide I) with transversal size reduction and simple setting is designed, which is fed by 50-Ω microstrip line, as shown in Fig. 3(a). It is composed of two parts: one is the periodic array containing five SSPP unit cells whose dimensions are the same as the ones in Fig. 1(b), and the other part is the gradient transition from microstrip line to SSPP periodic array with seamless connection. The two different lengths of the transition stubs h_1 and h_2 are set as 2.5 and 4 mm, respectively. The width of the 50-Ω microstrip line in this configuration is $w_0 = 1.54$ mm through calculation. The other parameters are selected as $l_0 = 5$ mm, $l_1 = 3$ mm.

As depicted in Fig. 3(b), due to the well-designed transition, the SSPP waveguide I has improved transmission (S_{21}) and reflection (S_{11}) performance. It realizes a lowpass filtering response with steep band edge. Within the passband, the return loss (RL) is higher than 10.3 dB, ensuring the stable and

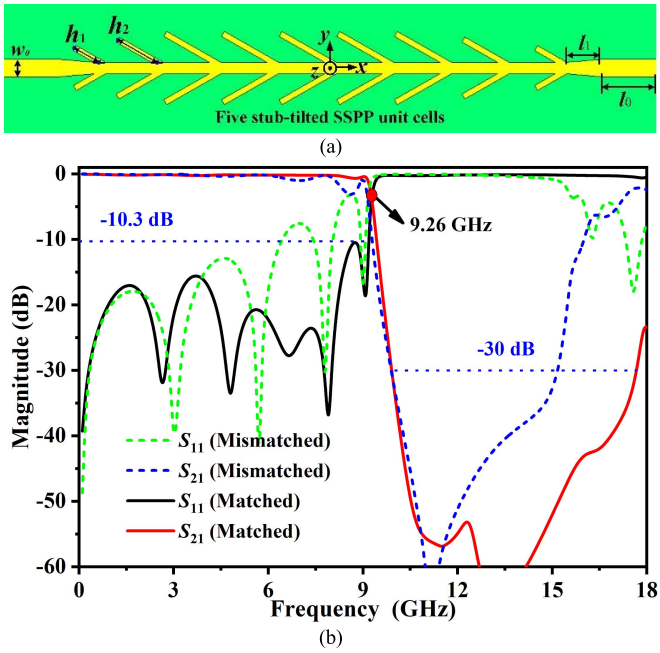

Fig. 3. (a) Sketch diagram of the SSPP waveguide I and (b) its simulated S-parameters along with the mismatched counterpart (i.e., SSPP waveguide I without transition part) for comparisons.

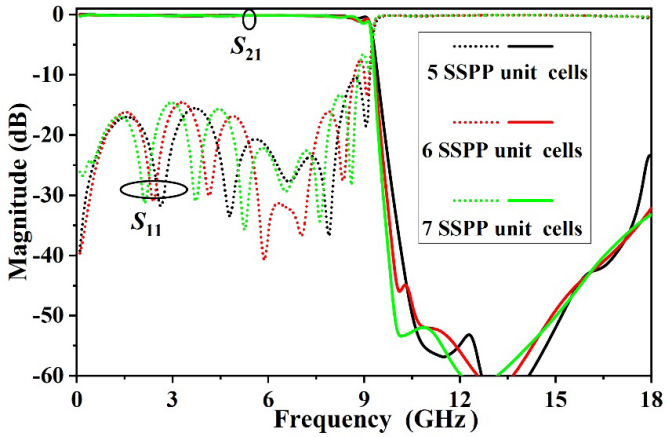

Fig. 4. Simulated S-parameters of the proposed SSPP waveguide I using different numbers of SSPP unit cells.

low-loss transmission passband. The 3-dB cutoff frequency of 9.26 GHz is marked, which almost agrees well with the asymptotic frequency of 9.31 GHz expected in the dispersion curve in Fig. 2. Meanwhile, at the stopband, the IL of 30 dB can reach up to 17.67 GHz, showing deep and wide rejection level. It should be noted that, although the SSPP waveguide I is asymmetrical in the longitudinal direction, there is no difference between S-parameters of S_{21} and S_{12} due to the reciprocity of passive circuit structure. Additionally, Fig. 4 exhibits the simulated S-parameters of SSPP waveguide I using different numbers of SSPP unit cells. With changing the number of SSPP unit cells, the whole transmission performance of the SSPP waveguide is almost unaffected.

To further study the propagation mechanism of SSPP waveguide I, the normalized electric field distributions at

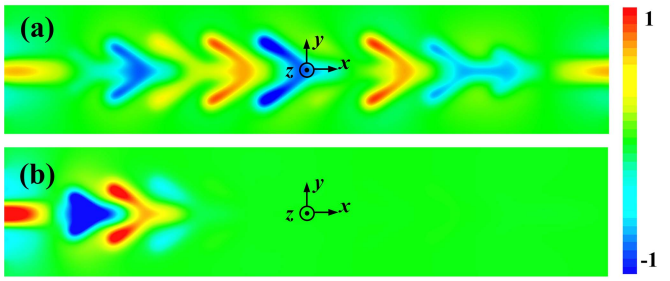

Fig. 5. Normalized electric field distributions at (a) 8 GHz and (b) 12 GHz on the xy plane above the SSPP waveguide I of 1 mm.

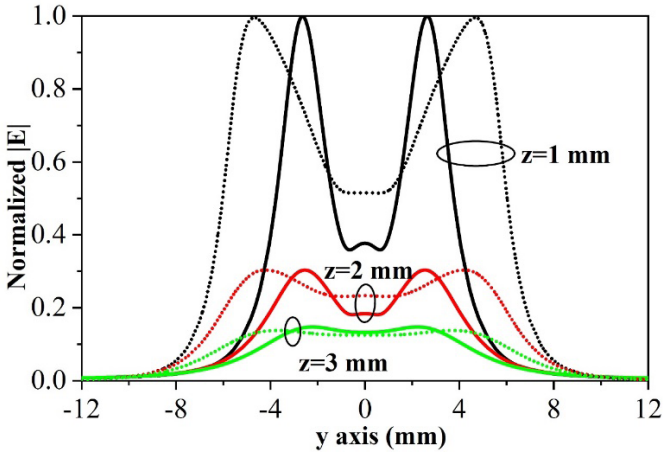

Fig. 6. Normalized electric fields $|E|$ along the y-axis at 8 GHz in the cases of $z = 1$ mm, $z = 2$ mm, and $z = 3$ mm, respectively, for the proposed SSPP waveguide I (solid line) and the conventional corrugated waveguide (short dotted line).

8 GHz (in-band) and 12 GHz (out-of-band) are presented in Fig. 5. It can be observed that, through the smooth transition, the SSPP mode is excited at 8 GHz, with the signals propagated from input to output port successfully. In contrast, due to SSPP mode is not induced at 12 GHz, the signal is blocked when transmitting along the waveguide. Fig. 6 illustrates the normalized electrical field $|E|$ along the y-axis at 8 GHz of SSPP waveguide I, as well as that of the conventional corrugated SSPP waveguide for comparison. Due to the $|E|$ varies along the x-axis, we choose the maximal $|E|$ position at $z = 1$ mm for both the two waveguides. As for z position, three cases of $z = 1$ mm, $z = 2$ mm, and $z = 3$ mm are selected. The $|E|$ of SSPP waveguide I and conventional SSPP waveguide are normalized to their own maximums. Due to the physical tilt, the SSPP waveguide I occupies less space, and the corresponding excited electric field energies are confined in smaller areas for these three cases. Additionally, observed from Fig. 6, the electrical fields are mostly concentrated on the end of two bilateral stubs in the case of $z = 1$, and become flat with z increases, for both of these two waveguides.

Furthermore, in contrast to the works having relatively large longitudinal sizes for a period of SSPP unit cell in [21]–[27], this approach can be applied in the case with small period value, which will facilitate the miniaturization of longitudinal size. To validate this, two SSPP waveguides with small periods of $p = 3$ mm and $p = 4$ mm will be investigated to compare with the one of $p = 5$ mm as analyzed above.

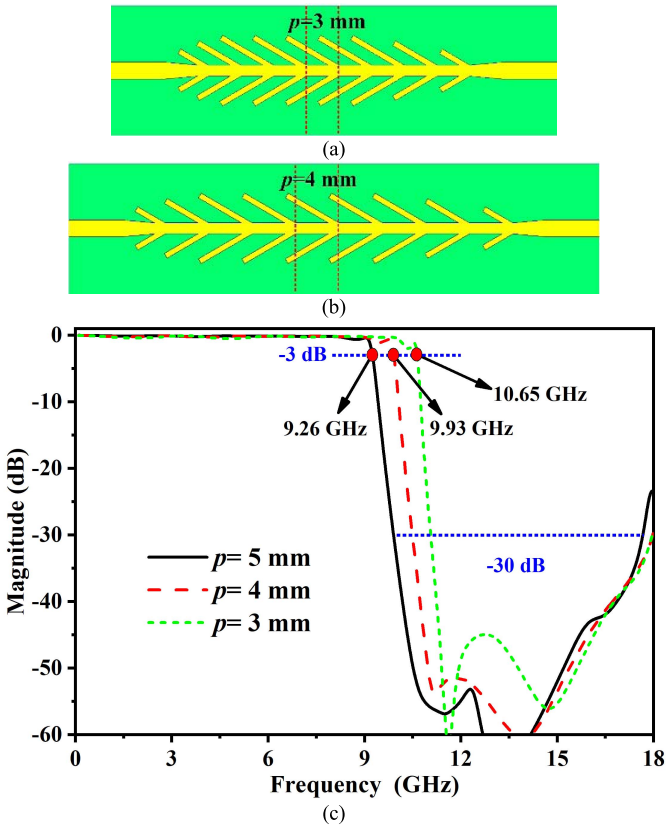

Fig. 7. Top view of the designed SSPP waveguides in small-period cases of (a) $p = 3$ mm and (b) $p = 4$ mm. The other parameters are the same as SSPP waveguide I. (c) Simulated transmission responses for the SSPP waveguide with different periods p.

Fig. 7(a) and (b) display the designed SSPP waveguides with $p = 3$ mm and $p = 4$ mm, respectively, where tilted stubs are overlapped with the closely spaced ones. Except the parameter "p," the two SSPP waveguides have same configurations with SSPP waveguide I, thus both of which have identical transversal sizes. Obviously, the longitudinal dimensions of these two SSPP waveguides are both reduced under the condition of same number of periodic unit cells. Fig. 7(c) illustrates the simulated transmission coefficients of the two SSPP waveguides, as well as that of the SSPP waveguide I for comparisons. It can be seen that the two SSPP waveguides with $p = 3$ mm and $p = 4$ mm also have good performance. The passband characteristic is very flat and the stopband rejection level is significantly high. Besides, the band edge becomes steeper as p decreases. In addition, with the decrease of p, the 3-dB cutoff frequency has a blue-shift due to the inherent property of the SSPP structure, which also exists in the conventional SSPP structure. Note that the transversal sizes of these two cases with $p = 3$ mm and $p = 4$ mm are still almost identical to that of the case with $p = 5$ mm. Therefore, this proposed approach is beneficial to the miniaturization design of planar plasmonic devices, both in transversal and longitudinal directions.

B. Improved SSPP Structure

Based on the stub-tilted SSPP unit cell featuring transversal size reduction as mentioned above, an improved SSPP unit cell is proposed to further decrease asymptotic frequency, as shown in the inset of Fig. 8, where the parameter a should be set smaller than the period p. It can be easily acquired by symmetrically adding additional stubs at the end of the tilted stubs with an intersection (red points in the inset of Fig. 8). When $h = 5$ mm and $\theta = 60°$, the transversal size occupation of stub part is $h_b = 2.78$ mm, slightly higher than that of the stub-tilted SSPP unit cell ($h_a = 2.72$ mm).

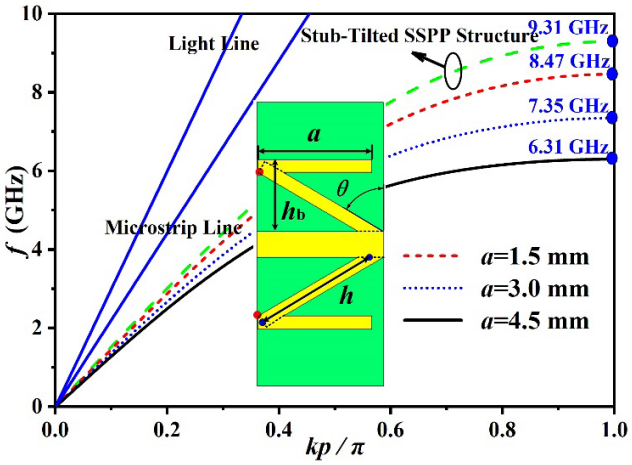

Fig. 8. Dispersion curves of the improved SSPP structure with different values of a, as well as that of the corresponding stub-tilted SSPP structure. The inset is the improved SSPP unit cell with the parameters of $\theta = 60°$, $h = 5$ mm, and $h_b = 2.78$ mm. The other parameters are identical to those in Fig. 1(b).

Fig. 8 presents the dispersion relations of the improved SSPP structure (i.e., periodic array of the improved SSPP unit cells) against different values of a, as well as that of the corresponding stub-tilted SSPP structure for comparisons. It is found that the improved SSPP structure has lower asymptotic frequency and stronger field confinement compared with its counterpart SSPP waveguide I. Additionally, the asymptotic frequency of this improved SSPP structure decreases from 8.47 to 6.31 GHz as the parameter a increases from 1.5 to 4.5 mm. Under the condition of same asymptotic frequency of 6.31 GHz, the improved SSPP structure with $a = 4.5$ mm occupies the whole transversal space of 6.56 mm, while the conventional SSPP structure needs the transversal space of 15.62 mm. Consequently, 58% reduction of transversal size can be realized.

Based on the proposed improved SSPP unit cell of $a = 4.5$ mm, a compact SSPP waveguide (SSPP waveguide II) is designed, fed by 50-Ω microstrip line, as shown in Fig. 9(a). In fact, SSPP waveguide II is constructed referring to SSPP waveguide I, by merely adding an additional transition part and substituting the stub-tilted SSPP unit cells with improved SSPP unit cells. The new adding transition part has the parameters of $a_1 = 3$ mm and $h_3 = 5$ mm. The other parameters are the same as the SSPP waveguide I in Fig. 3(a). It is worth mentioning that the SSPP waveguide II not only has a simple configuration, but also can realize the transversal size reduction of 58% compared with the conventional corrugated SSPP waveguide.

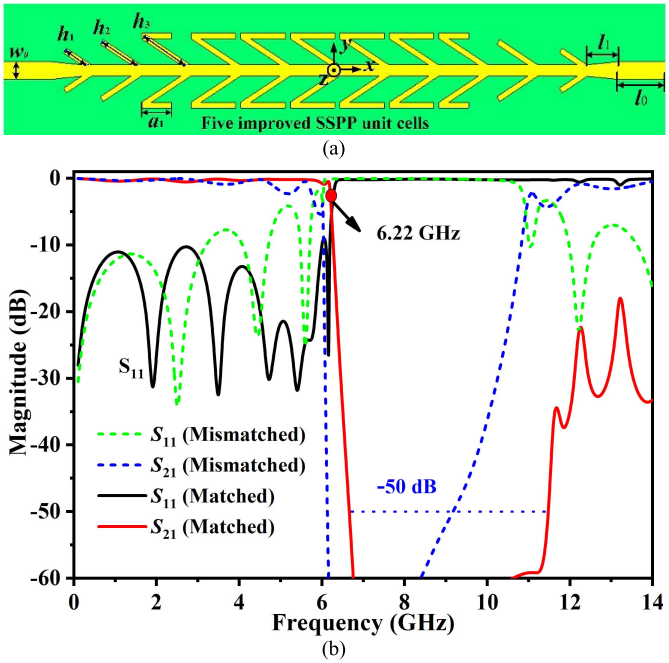

Fig. 9. (a) Schematic configuration of SSPP waveguide II and (b) its simulated S-parameters along with the mismatched counterpart (i.e., SSPP waveguide II without transition part) for comparisons.

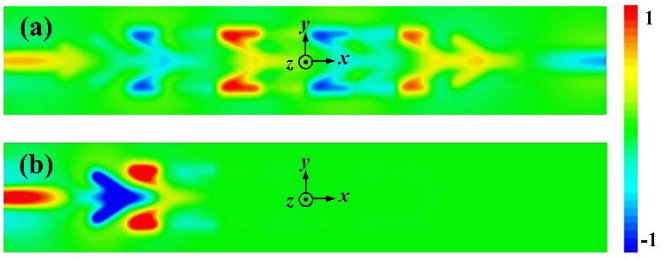

Fig. 10. Normalized electric field distributions at (a) 5 GHz and (b) 8 GHz on the xy plane above the compact SSPP waveguide II of 1 mm.

The compact SSPP waveguide II is investigated by the frequency domain solver simulation, and its simulated S-parameters are displayed in Fig. 9(b). It can be seen that the SSPP waveguide II has improved S-parameters due to the addition of the well-designed transition part. The 3-dB cutoff frequency of 6.22 GHz is marked, which reasonably agrees well with the asymptotic frequency of 6.31 GHz as predicted in dispersion curve. The flat passband and steep band-edge are achieved, together with the rejection level of 50 dB at stopband up to 11.48 GHz. Also, the unwanted spurious band at about 11–14 GHz is effectively suppressed, resulting in wide stopband.

Fig. 10 illustrates the normalized electric field distributions of SSPP waveguide II at 5 and 8 GHz, which are located in passband and stopband, respectively. Obviously, the electric fields at 5 GHz mainly concentrated on the metallic strips can transmit through the SSPP waveguide II due to the excited SSPP mode propagation, while the electric fields at 8 GHz are blocked at the transition part with high electric field intensity. Additionally, Fig. 11 illustrates the normalized electrical field

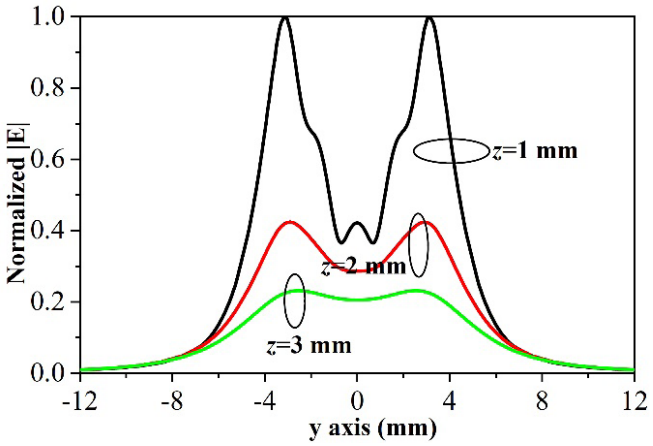

Fig. 11. Normalized electric fields $|E|$ along the y-axis at 5 GHz in the cases of $z = 1$ mm, $z = 2$ mm, and $z = 3$ mm, respectively, for the proposed SSPP waveguide II.

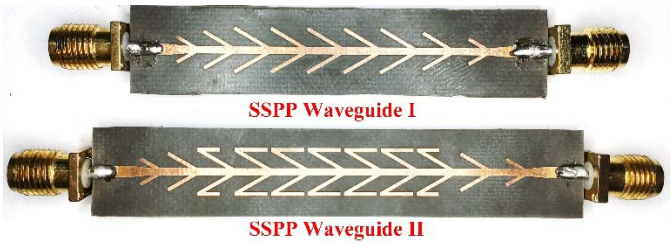

Fig. 12. Photographs of two fabricated SSPP waveguides.

$|E|$ along the y-axis at 5 GHz in the cases of $z = 1$ mm, $z = 2$ mm, and $z = 3$ mm, respectively, for the proposed SSPP waveguide II. The $|E|$ of the SSPP waveguide II is extracted at $x = -2$ mm (i.e., the center position of the middle SSPP unit cell). Moreover, the $|E|$ is normalized to its maximum. It is clear that the $|E|$ at $z = 1$ mm is mostly concentrated on the two additional stubs, and becomes flat as z increases, similar to the SSPP waveguide I.

III. Experimental Verification

In order to demonstrate the feasibility of our design, two above-mentioned prototypes, SSPP waveguides I and II, are fabricated. Fig. 12 exhibits the top view of the two fabricated SSPP waveguides. The back of them is covered by metal as the ground. The SubMiniature version A (SMA) connectors are welded to the ends of them for ease of measurement.

Fig. 13 presents the measured results, including the S-parameters and group delay, which have good agreement with the simulated ones. According to the results, both the two samples have excellent passband, such as low IL and good RL of over 10.3 dB. Especially for SSPP waveguide I, its passband is flat with the IL of better than 0.5 dB. Moreover, the roll-off rate at band-edge keeps well, especially for SSPP waveguide II. Note that the measured performance of the two SSPP waveguides deteriorates slightly when the frequency is higher than 13 GHz, which may be caused by the external disturbance due to no shielding cavities used for measurement. Additionally, the group delays of the two SSPP waveguides are

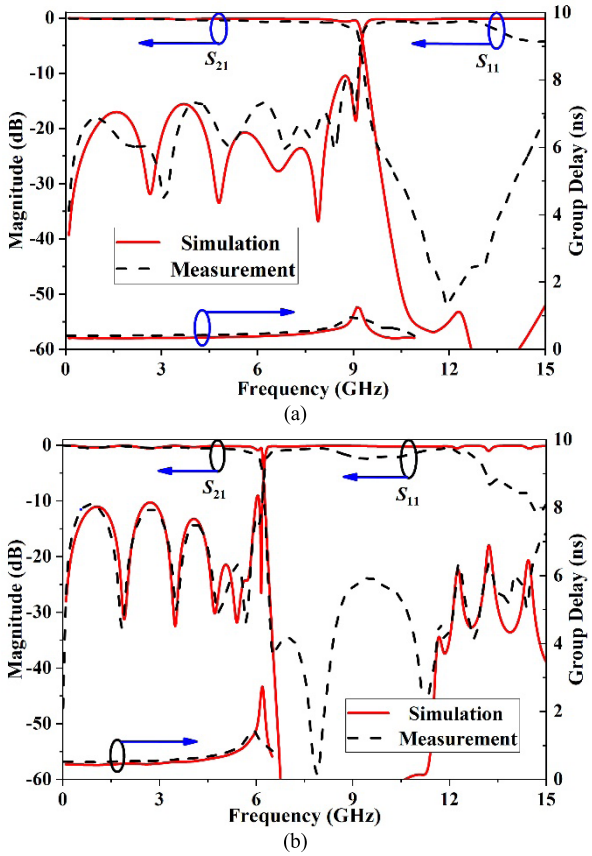

Fig. 13. Measured results of (a) SSPP waveguide I and (b) SSPP waveguide II along with the corresponding simulated results.

TABLE I
COMPARISONS WITH SOME PREVIOUS WORKS

	IL (dB)	RL (dB)	Type	Transversal size reduction compared with conventional ones
[26]	3.2	10	Bandpass	55.2%
[27]	1.1	11	Bandpass	Around 75%
[28]	1	15	Lowpass	Around 50%
[30]-I	Around 3	Around 8	Lowpass	33%
[30]-II	Around 3	Around 8	Lowpass	53%
This work-I	**0.5**	**10.3**	**Lowpass**	**33%**
This work-II	**0.5**	**10.5**	**Lowpass**	**58%**

flat within lowpass band. Table I tabulates the performance comparisons with some previous works, which indicates that the two proposed SSPPs possess low ILs, good RLs, and miniaturized sizes. In summary, the two compact experimental prototypes with transversal size reductions and good performance have validated our design idea successfully.

IV. CONCLUSION

In this article, two compact SSPP waveguides with simple configurations and good performance have been presented, and the transversal size reductions have been achieved. The properties of these two SSPP waveguides have been analyzed in detail. Good agreement between the simulated and measured results validates the feasibility and potential of our designs. The presented works will be of great benefit for the development of miniaturized plasmonic devices and circuits at microwave or terahertz frequencies.

REFERENCES

[1] W. L. Barnes, A. Dereux, and T. W. Ebbesen, "Surface plasmon subwavelength optics," *Nature*, vol. 424, no. 6950, pp. 824–830, 2003.
[2] J. M. Pitarke, V. M. Silkin, E. V. Chulkov, and P. M. Echenique, "Theory of surface plasmons and surface-plasmon polaritons," *Rep. Prog. Phys.*, vol. 70, pp. 1–87, Dec. 2006.
[3] E. Ozbay, "Plasmonics: Merging photonics and electronics at nanoscale dimensions," *Science*, vol. 311, no. 5758, pp. 189–193, Jan. 2006.
[4] D. K. Gramotnev and S. I. Bozhevolnyi, "Plasmonics beyond the diffraction limit," *Nature Photon.*, vol. 4, no. 2, pp. 83–91, 2010.
[5] J. B. Pendry, L. Martín-Moreno, and F. J. Garcia-Vidal, "Mimicking surface plasmons with structured surfaces," *Science*, vol. 305, no. 5685, pp. 847–848, Aug. 2004.
[6] C. R. Williams, S. R. Andrews, S. A. Maier, A. I. Fernández-Domínguez, L. Martín-Moreno, and F. J. García-Vidal, "Highly confined guiding of terahertz surface plasmon polaritons on structured metal surfaces," *Nature Photon.*, vol. 2, pp. 175–179, Mar. 2008.
[7] K.-D. Xu *et al.*, "On-chip GaAs-based spoof surface plasmon polaritons at millimeter-wave regime," *IEEE Photon. Technol. Lett.*, vol. 33, no. 5, pp. 255–258, Mar. 1, 2021.
[8] L. Pan, Y. Wu, W. Wang, Y. Wei, and Y. Yang, "A flexible high-selectivity single-layer coplanar waveguide bandpass filter using interdigital spoof surface plasmon polaritons of bow-tie cells," *IEEE Trans. Plasma Sci.*, vol. 48, no. 10, pp. 3582–3588, Oct. 2020.
[9] Y.-J. Guo, K.-D. Xu, X. Deng, X. Cheng, and Q. Chen, "Millimeter-wave on-chip bandpass filter based on spoof surface plasmon polaritons," *IEEE Electron Device Lett.*, vol. 41, no. 8, pp. 1165–1168, Aug. 2020.
[10] W. Feng, Y. Feng, Y. Shi, S. Shi, and W. Che, "Novel differential bandpass filter using spoof surface plasmon polaritons," *IEEE Trans. Plasma Sci.*, vol. 48, no. 6, pp. 2083–2088, Jun. 2020.
[11] K.-D. Xu, S. Lu, Y.-J. Guo, and Q. Chen, "High-order mode of spoof surface plasmon polaritons and its application in bandpass filters," *IEEE Trans. Plasma Sci.*, vol. 49, no. 1, pp. 269–275, Jan. 2021.
[12] Y. Liu, K.-D. Xu, Y.-J. Guo, and Q. Chen, "High-order mode application of spoof surface plasmon polaritons in bandpass filter design," *IEEE Photon. Technol. Lett.*, vol. 33, no. 7, pp. 362–365, Apr. 1, 2021.
[13] L. Ji, X.-C. Li, X. He, and J.-F. Mao, "A slow wave ridged half-mode substrate integrated waveguide with spoof surface plasmon polaritons," *IEEE Trans. Plasma Sci.*, vol. 49, no. 6, pp. 1818–1825, Jun. 2021.
[14] Y. Wu *et al.*, "A new self-packaged substrate integrated air-filled spoof surface plasmon polaritons line with inherent low loss and deep upper frequency suppression," *IEEE Trans. Plasma Sci.*, vol. 48, no. 10, pp. 3516–3523, Oct. 2020.
[15] Y. Wei, Y. Wu, W. Wang, L. Pan, Y. Yang, and Y. Liu, "Double-sided spoof surface plasmon polaritons- line bandpass filter with excellent dual-band filtering and wide upper band suppressions," *IEEE Trans. Plasma Sci.*, vol. 48, no. 12, pp. 4134–4143, Dec. 2020.
[16] D.-F. Guan, P. You, Q. Zhang, Z.-H. Lu, S.-W. Yong, and K. Xiao, "A wide-angle and circularly polarized beam-scanning antenna based on microstrip spoof surface plasmon polariton transmission line," *IEEE Antennas Wireless Propag. Lett.*, vol. 16, pp. 2538–2541, 2017.
[17] W. Feng, Y. Feng, W. Yang, W. Che, and Q. Xue, "High-performance filtering antenna using spoof surface plasmon polaritons," *IEEE Trans. Plasma Sci.*, vol. 47, no. 6, pp. 2832–2837, Jun. 2019.
[18] W. Feng, Y. Feng, L.-S. Wu, Y. Shi, X. Y. Zhou, and W. Che, "A novel leaky wave endfire filtering antenna based on spoof surface plasmon polaritons," *IEEE Trans. Plasma Sci.*, vol. 48, no. 7, pp. 3061–3066, Sep. 2020.
[19] B. Qu, S. Yan, A. Zhang, Y. Pang, and Z. Xu, "Miniaturization of monopole antenna based on spoof surface plasmon polaritons," *IEEE Antennas Wireless Propag. Lett.*, vol. 20, no. 8, pp. 1562–1566, Aug. 2021.
[20] C. Han, Z. H. Wang, Y. Y. Chu, X. D. Zhao, and X. R. Zhang, "Compact flexible multifrequency splitter based on plasmonic graded metallic grating arc waveguide," *Opt. Lett.*, vol. 43, no. 8, pp. 1898–1901, 2018.
[21] J. Wang, L. Zhao, Z. C. Hao, X. P. Shen, and T. J. Cui, "Splitting spoof surface plasmon polaritons to different directions with high efficiency in ultra-wideband frequencies," *Opt. Lett.*, vol. 44, no. 13, pp. 3374–3377, Jul. 2019.

[22] M. A. Unutmaz and M. Unlu, "Fixed physical length spoof surface plasmon polariton delay delay lines for a 2-bit phase shifter," *J. Opt. Soc. Amer. B, Opt. Phys.*, vol. 37, no. 4, pp. 1116–1121, 2020.
[23] Q. Le Zhang, B. J. Chen, K.-M. Shum, and C. H. Chan, "Ultra-wideband and compact terahertz planar load based on spoof surface plasmon polaritons with nickel," *IEEE Trans. Circuits Syst. II, Exp. Briefs*, vol. 68, no. 6, pp. 1922–1926, Jun. 2021, doi: 10.1109/TCSII.2020.3043800.
[24] K. D. Xu, Y. J. Guo, and X. Deng, "Terahertz broadband spoof surface plasmon polaritons using high-order mode developed from ultra-compact split-ring grooves," *Opt. Exp.*, vol. 27, no. 4, pp. 4354–4363, Feb. 2019.
[25] L. Ye *et al.*, "Super subwavelength guiding and rejecting of terahertz spoof SPPs enabled by planar plasmonic waveguides and notch filters based on spiral-shaped units," *J. Lightw. Technol.*, vol. 36, no. 20, pp. 4988–4994, Oct. 15, 2018.
[26] K.-D. Xu, F. Zhang, Y. Guo, L. Ye, and Y. Liu, "Spoof surface plasmon polaritons based on balanced coplanar stripline waveguides," *IEEE Photon. Technol. Lett.*, vol. 32, no. 1, pp. 55–58, Jan. 1, 2020.
[27] M. Wang, S. Sun, H. F. Ma, and T. J. Cui, "Supercompact and ultrawideband surface plasmonic bandpass filter," *IEEE Trans. Microw. Theory Techn.*, vol. 68, no. 2, pp. 732–740, Feb. 2020.
[28] L. Ye, Y. Chen, Z. Wang, C. Zhu, J. Zhuo, and Q. H. Liu, "Compact spoof surface plasmon polariton waveguides and notch filters based on meander-strip units," *IEEE Photon. Technol. Lett.*, vol. 33, no. 3, pp. 135–138, Feb. 1, 2021.
[29] L. Ye, H. Feng, W. Li, and Q. H. Liu, "Ultra-compact spoof surface plasmon polariton waveguides and notch filters based on double-sided parallel-strip lines," *J. Phys. D: Appl. Phys.*, vol. 53, no. 26, Jun. 2020, Art. no. 265502.
[30] Z. Shi, Y. Shen, and S. Hu, "Spoof surface plasmon polariton transmission line with reduced line-width and enhanced field confinement," *Int. J. RF Microw. Comput.-Aided Eng.*, vol. 30, no. 8, Aug. 2020, Art. no. e22276.

Sen Lu (Student Member, IEEE) was born in Shandong, China, in 1996. He received the B.Eng. degree from Northeastern University, Qinhuangdao, China, in 2018, and the M.Eng. degree from Xiamen University, Xiamen, China, in 2021. He is currently pursuing the Ph.D. degree with the State Key Laboratory of Millimeter Waves, School of Information Science and Engineering, Southeast University, Nanjing, China.

His research interests include RF and microwave passive components.

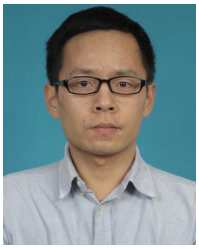

Kai-Da Xu (Senior Member, IEEE) received the B.E. and Ph.D. degrees in electromagnetic field and microwave technology from the University of Electronic Science and Technology of China (UESTC), Chengdu, China, in 2009 and 2015, respectively.

From 2012 to 2014, he was a Visiting Researcher with the Department of Electrical and Computer Engineering, Duke University, Durham, NC, USA, under the financial support from the China Scholarship Council. In 2015, he joined the Department of Electronic Science, Xiamen University, Xiamen, China, as an Assistant Professor. From 2016 to 2017, he was a Post-Doctoral Fellow with the State Key Laboratory of Millimeter Waves, City University of Hong Kong, Hong Kong. From 2018 to 2019, he was a Honorary Fellow with the Department of Electrical and Computer Engineering, University of Wisconsin–Madison, Madison, WI, USA. He was successfully selected into the "Youth Talent Support Program" of Xi'an Jiaotong University (XJTU), Xi'an, China, in May 2019, and joined the School of Information and Communications Engineering, XJTU, in January 2020. He has authored or coauthored more than 120 articles in peer-reviewed journals and more than 40 papers in conference proceedings. His current research interests include RF/microwave, millimeter-wave/terahertz (THz) devices and antenna arrays.

Dr. Xu was awarded a fellowship from the Japan Society for the Promotion of Science (JSPS) and the JSPS Fellow with the Department of Communications Engineering, Graduate School of Engineering, Tohoku University, Sendai, Japan, from November 2019 to May 2021. He was a recipient of the UESTC Outstanding Graduate Awards in 2009 and 2015 and the National Graduate Student Scholarship in 2012, 2013, and 2014 from the Ministry of Education, China. Since 2017, he has been an Associate Editor for both the IEEE ACCESS and *Electronics Letters*. He has also served as an Editorial Board Member for both the *AEÜ-International Journal of Electronics and Communications* and *MDPI Electronics*.

Ying-Jiang Guo (Member, IEEE) received the B.E. degree in electronic engineering from Sichuan University, Chengdu, China, in 2008, and the Ph.D. degree in electronic engineering from the University of Electronic Science and Technology of China, Chengdu, in 2018.

From 2011 to 2013, he was with Huawei Technologies Company, Ltd., Shenzhen, China, where he was involved in the research of 5G communication prototype design. From 2013 to 2014, he was with Sichuan Normal University, Chengdu, as a Lecturer. Since 2018, he has been with the Microsystem and Terahertz Research Center, China Academy of Engineering Physics, Chengdu, as an Assistant Research Fellow and focuses on the terahertz (THz) integrated circuits and communication technologies. He has authored or coauthored more than 30 journal articles and conference papers. He holds five patents in wireless communication. His research interests include the RF/microwave/millimeter-wave integrated circuits, THz modules/antennas, and systems in package.

Qiang Chen (Senior Member, IEEE) received the B.E. degree from Xidian University, Xi'an, China, in 1986, and the M.E. and D.E. degrees from Tohoku University, Sendai, Japan, in 1991 and 1994, respectively.

He is currently the Chair Professor with the Electromagnetic Engineering Laboratory, Department of Communications Engineering, School of Engineering, Tohoku University. His primary research interests include antennas, microwave and millimeter-wave, antenna measurement and computational electromagnetics.

Dr. Chen is an Institute of Electronics, Information and Communication Engineers (IEICE) Fellow. He was a recipient of the Best Paper Award and the Zen-ichi Kiyasu Award in 2009 from the IEICE. He served as the Chair of IEICE Technical Committee on Photonics-applied Electromagnetic Measurement from 2012 to 2014, the Chair of IEICE Technical Committee on Wireless Power Transfer from 2016 to 2018, and the Chair of Tokyo Chapter of IEEE Antennas and Propagation Society from 2017 to 2018. He is currently the Chair of IEICE Technical Committee on Antennas and Propagation.